
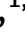



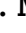






# Spike propagation mapping reveals effective connectivity and predicts surgical outcome in epilepsy

 Margherita A. G. Matarrese,<sup>1,2,3</sup>  Alessandro Loppini,<sup>2</sup>  Lorenzo Fabbri,<sup>1,3</sup>  
 Eleonora Tamilia,<sup>4</sup>  M. Scott Perry,<sup>1</sup>  Joseph R. Madsen,<sup>5</sup>  Jeffrey Bolton,<sup>6</sup>  
Scellig S. D. Stone,<sup>5</sup>  Phillip L. Pearl,<sup>6</sup>  Simonetta Filippi<sup>2</sup> and  Christos Papadelis<sup>1,3,7</sup>

Neurosurgical intervention is the best available treatment for selected patients with drug resistant epilepsy. For these patients, surgical planning requires biomarkers that delineate the epileptogenic zone, the brain area that is indispensable for the generation of seizures. Interictal spikes recorded with electrophysiological techniques are considered key biomarkers of epilepsy. Yet, they lack specificity, mostly because they propagate across brain areas forming networks. Understanding the relationship between interictal spike propagation and functional connections among the involved brain areas may help develop novel biomarkers that can delineate the epileptogenic zone with high precision. Here, we reveal the relationship between spike propagation and effective connectivity among onset and areas of spread and assess the prognostic value of resecting these areas.

We analysed intracranial EEG data from 43 children with drug resistant epilepsy who underwent invasive monitoring for neurosurgical planning. Using electric source imaging, we mapped spike propagation in the source domain and identified three zones: onset, early-spread and late-spread. For each zone, we calculated the overlap and distance from surgical resection. We then estimated a virtual sensor for each zone and the direction of information flow among them via Granger causality. Finally, we compared the prognostic value of resecting these zones, the clinically-defined seizure onset zone and the spike onset on intracranial EEG channels by estimating their overlap with resection.

We observed a spike propagation in source space for 37 patients with a median duration of 95 ms (interquartile range: 34–206), a spatial displacement of 14 cm (7.5–22 cm) and a velocity of 0.5 m/s (0.3–0.8 m/s). In patients with good surgical outcome (25 patients, Engel I), the onset had higher overlap with resection [96% (40–100%)] than early-spread [86% (34–100%),  $P = 0.01$ ] and late-spread [59% (12–100%),  $P = 0.002$ ], and it was also closer to resection than late-spread [5 mm versus 9 mm,  $P = 0.007$ ]. We found an information flow from onset to early-spread in 66% of patients with good outcomes, and from early-spread to onset in 50% of patients with poor outcome. Finally, resection of spike onset, but not area of spike spread or the seizure onset zone, predicted outcome with positive predictive value of 79% and negative predictive value of 56% ( $P = 0.04$ ).

Spatiotemporal mapping of spike propagation reveals information flow from onset to areas of spread in epilepsy brain. Surgical resection of the spike onset disrupts the epileptogenic network and may render patients with drug resistant epilepsy seizure-free without having to wait for a seizure to occur during intracranial monitoring.

1 Jane and John Justin Institute for Mind Health Neurosciences Center, Cook Children's Health Care System, Fort Worth, TX, USA

2 Laboratory of Nonlinear Physics and Mathematical Modeling, Department of Engineering, Università Campus Bio-Medico di Roma, Rome, Italy

- 3 Department of Bioengineering, The University of Texas at Arlington, Arlington, TX, USA
- 4 Fetal-Neonatal Neuroimaging and Developmental Science Center, Boston Children's Hospital, Harvard Medical School, Boston, MA, USA
- 5 Division of Epilepsy Surgery, Department of Neurosurgery, Boston Children's Hospital, Harvard Medical School, Boston, MA, USA
- 6 Division of Epilepsy and Clinical Neurophysiology, Department of Neurology, Boston Children's Hospital, Harvard Medical School, Boston, MA, USA
- 7 School of Medicine, Texas Christian University, Fort Worth, TX, USA

Correspondence to: Christos Papadelis

Director of Research, Jane and John Justin Neurosciences Center

Cook Children's Health Care System, 1500 Cooper St., Fort Worth, TX, 76104, USA

E-mail: christos.papadelis@cookchildrens.org

**Keywords:** electric source imaging; spike propagation; epilepsy biomarkers; epilepsy surgery; effective connectivity; inverse problem

## Introduction

Approximately 20–30% of patients with epilepsy are unable to control their seizures with antiepilepsy medications and suffer from drug resistant epilepsy (DRE).<sup>1</sup> For these patients, neurosurgery offers ~50% chance to achieve seizure freedom.<sup>2–4</sup> Yet, it remains an underutilized treatment, particularly for children who may benefit the most since their brain possesses extensive neuroplasticity and thus the opportunity to be rewired after surgery. The success of epilepsy surgery depends heavily upon precision and accuracy in resecting the epileptogenic zone (EZ).<sup>5</sup> To date, there is no clinical exam to delineate the EZ unambiguously. Instead, the EZ is defined ambiguously based on multiple diagnostic tests.<sup>6</sup>

The most established biomarker for the EZ is the seizure onset zone (SOZ) as defined by intracranial EEG (iEEG).<sup>5,7</sup> However, iEEG implantation has limited spatial sampling, since it is blind to brain areas that are not in close proximity to electrodes.<sup>8</sup> This makes it hard to judge whether a recorded seizure onset represents the actual onset generator or propagation from other regions.<sup>9</sup> Thus, the EZ may be missed, leading to unsuccessful surgery. Moreover, the SOZ may not represent the full EZ extent, and its delineation requires recording several stereotyped seizures at the expense of considerable human and financial resources.<sup>10</sup> Thus, there is a need for an interictal biomarker that can delineate the EZ with higher spatial resolution than iEEG without having to wait for a seizure to occur.<sup>11</sup>

Spikes are regarded as the most established interictal biomarkers of epilepsy.<sup>12</sup> However, they suffer from low specificity to the EZ because the area they define is often larger than the EZ and thus may overlap with eloquent areas that should be preserved.<sup>13</sup> Currently, spike detection is performed on individual iEEG contacts independently from neighbouring electrodes. Yet, spikes do not occur only as 'isolated' events in single contacts each time; instead, they are often seen in multiple contacts at a time with a specific spatial displacement and duration.<sup>14–18</sup> Like seizures, spikes often propagate rapidly across the cortex reaching locations far from onset.<sup>16,18</sup> The onset of this propagating activity correlates with the SOZ, and its removal is associated with good surgical outcome.<sup>19,20</sup> Yet, the neuropathology of this mechanism remains elusive.<sup>18,19,21</sup> Intracranial EEG may help investigate spike propagation but its intrinsic limited spatial resolution could result in misleading localization of the onset since the location of the recording contacts may differ from the actual source of recorded activity.<sup>22</sup> Electrical source imaging (ESI) performed on interictal iEEG may improve the

spatiotemporal mapping of spike propagation overcoming iEEG limitations and facilitating EZ delineation.<sup>22–25</sup>

Epilepsy is increasingly seen as a brain disorder of networks.<sup>26,27</sup> Studying these networks with functional connectivity (FC) can help identify hubs that facilitate the spread of epileptiform activity.<sup>28–30</sup> Surgical resection, focal ablation, or neuromodulation of these hubs may lead to seizure freedom in patients suffering from DRE.<sup>31,32</sup> Several iEEG studies report high interictal FC within resection in patients with DRE and favourable outcome,<sup>31–34</sup> but the findings are considerably heterogeneous.<sup>35,36</sup> Moreover, FC does not provide any information regarding the directionality of information flow (e.g. effective connectivity) that is critical for studying propagation phenomena.<sup>37,38</sup> Thus, information flow between different brain regions remains largely unknown.<sup>39–41</sup> Completely unexplored is also the relationship between propagating epileptic activity and information flow among onset and areas of spread. Mapping information flow of propagating activity may help us understand the functional architecture of epileptogenic networks, allowing selective disruption of critical hubs that may render patients seizure free.

Here, we aim to map the spatiotemporal propagation of spikes across the brains of children with DRE, estimate the information flow among the onset and areas of spread, reveal the relationship between information flow and propagation among these areas, and assess the prognostic value of resecting these areas. We hypothesize that information flows outwards from onset to areas of spread and resection of onset areas disrupts the pathological network, predicting outcome better than resecting areas of spread. To test our hypothesis, we assessed the spatiotemporal propagation of spikes with ESI and identified three regions (or zones) of interest: 'onset', 'early-spread' and 'late-spread'. We then estimated virtual sensors within each zone and computed the effective connectivity among them with Granger causality (GC).<sup>41</sup> We also estimated the overlap of each zone with resection to test whether its removal predicts outcome. Finally, we evaluated information flow among these zones to assess whether they follow a hierarchical epileptogenic organization (i.e. epileptogenic activity flows from the onset to early-spread, and finally to the late-spread zone).

## Materials and methods

### Subjects selection

We retrospectively investigated patients with DRE who had long-term monitoring (LTM) with iEEG and consequent resective

neurosurgery at Boston Children's Hospital between July 2012 and June 2018. We included patients who met the following criteria: (i) LTM with a subdural electrocorticography (ECoG) grid, strips and/or stereoelectroencephalography (sEEG) depth electrodes; (ii) pre- and post-surgical MRI and post-implant CT; (iii) SOZ defined by clinicians in the presurgical phase; and (iv) availability of surgical outcome at least 1 year after surgery. The study was approved by our Institutional Review Board.

### Structural imaging and intracranial EEG recordings

We employed MRI and CT to obtain structural information for each patient. We used the pre-implant MRI space as a reference space to rotate and reslice the post-implant CT (voxel size =  $0.5 \times 0.5 \times 0.5$  mm<sup>3</sup>) and post-surgical MRI with Brainstorm.<sup>42</sup> We segmented the preoperative MRI and reconstructed the patient-specific 3D cortical surface via FreeSurfer.<sup>43</sup> We recorded iEEG data from each patient for several days with XLTEK NeuroWorks (Natus Inc.). The sampling rate ranged from 0.5 to 2 kHz. We defined the implanted electrode positions (Fig. 1A) through a co-registration procedure described previously.<sup>44</sup> We identified 5-min epochs from non-REM slow-wave sleep (when this was possible) given the highest spike rate<sup>45</sup> and minimal presence of motion artifacts in the recordings during these stages. Epochs were selected to be at least 1 h after/before a clinical seizure or half an hour after/before an electrographic seizure.<sup>46</sup>

### Resection, seizure onset zone and outcome

Paediatric epileptologists defined the SOZ through visual review of all segments with ictal activity independently from this study. The iEEG contact(s) that first showed a change of activity associated with clinical seizures was/were considered part of the SOZ. We then defined the SOZ as the tissue surrounding each iEEG location up to 10 mm from the centre of each contact. The 10 mm cut-off selection was based on previous studies showing that the gyral width ranges from 11 to 21 mm<sup>47–49</sup>; thus, we presumed that sources located within 10 mm of the SOZ (or resection) belong to the same gyrus. Resection volume was obtained by marking the post-surgical cavity's edges on the preoperative MRIs.<sup>42</sup>

Patient outcome was assessed during a follow-up visit at least 1 year after surgery using the Engel classification (classes I–IV).<sup>50</sup> We then dichotomized patients into having good (Engel IA–D) or poor (Engel ≥II) outcome.

### Spike detection and propagation

We performed detection of spikes using Persyst 14.0 (Persyst Development).<sup>51</sup> Detection was performed separately for each channel on segments that were initially preprocessed (common average reference, DC removal, band-pass between 1–70 and 60 Hz notch). Previous findings reported statistical non-inferiority of Persyst compared to human readers in terms of sensitivity and false positive rate.<sup>51</sup> To ensure robustness of findings, we examined the performance of Persyst automated marking in data from five patients in our cohort by comparing them with manual reading of one EEG expert (C.P.) and obtaining 85% of sensitivity and 72% of precision. We further performed manual inspection and correction of all automated markings for all patients. We categorized spikes as either 'isolated' or 'propagating events' using an in-house algorithm. We defined propagating events as spike sequences that involved at least three channels (Fig. 1A)<sup>48,52</sup>; all other spikes were regarded as isolated.

### Intracranial EEG source imaging

For each patient, we constructed a forward model with boundary element method using OpenMEEG.<sup>53</sup> Source space included one or both hemispheres depending on the implanted electrodes' locations (Fig. 1B). For each propagating event, we solved the inverse problem using dynamic statistical parametric mapping (dSPM)<sup>54</sup> obtaining spatiotemporal unconstrained dipole maps of time windows with 500 ms duration (from –200 to 300 ms, with 0 corresponding to the first onset spike) using Brainstorm (Fig. 1B). This duration was selected to capture the entire propagation phenomenon, based on prior findings showing a maximum duration of 250 ms.<sup>18,19,21</sup> We considered the data covariance matrix to be all windows centred around each spike's onset with a 200 ms duration, and the noise covariance to be the identity matrix. To reduce the source spurious activity, we considered windows with a correlation above 0.7 between the reconstructed and original signal. We averaged all dipole maps corresponding to the different propagation events in the source space to obtain a unique map for each patient. Each map contained three components corresponding to the three orthogonal dipoles at each grid location. We then computed each source's amplitude along these components and normalized this map with respect to its activation's maximum value. This resulting map ( $S_{\text{map}}$ ) was a normalized  $N \times M$  matrix, where  $N$  is the number of sources and  $M$  is the number of samples. Finally, we averaged each 5 ms window to regularize the sources activity of  $S_{\text{map}}$  and create a volumetric region of activation (VRA) for each interval. The temporal evolution of VRAs was defined as the ESI spike propagation for that specific patient (Fig. 1C).

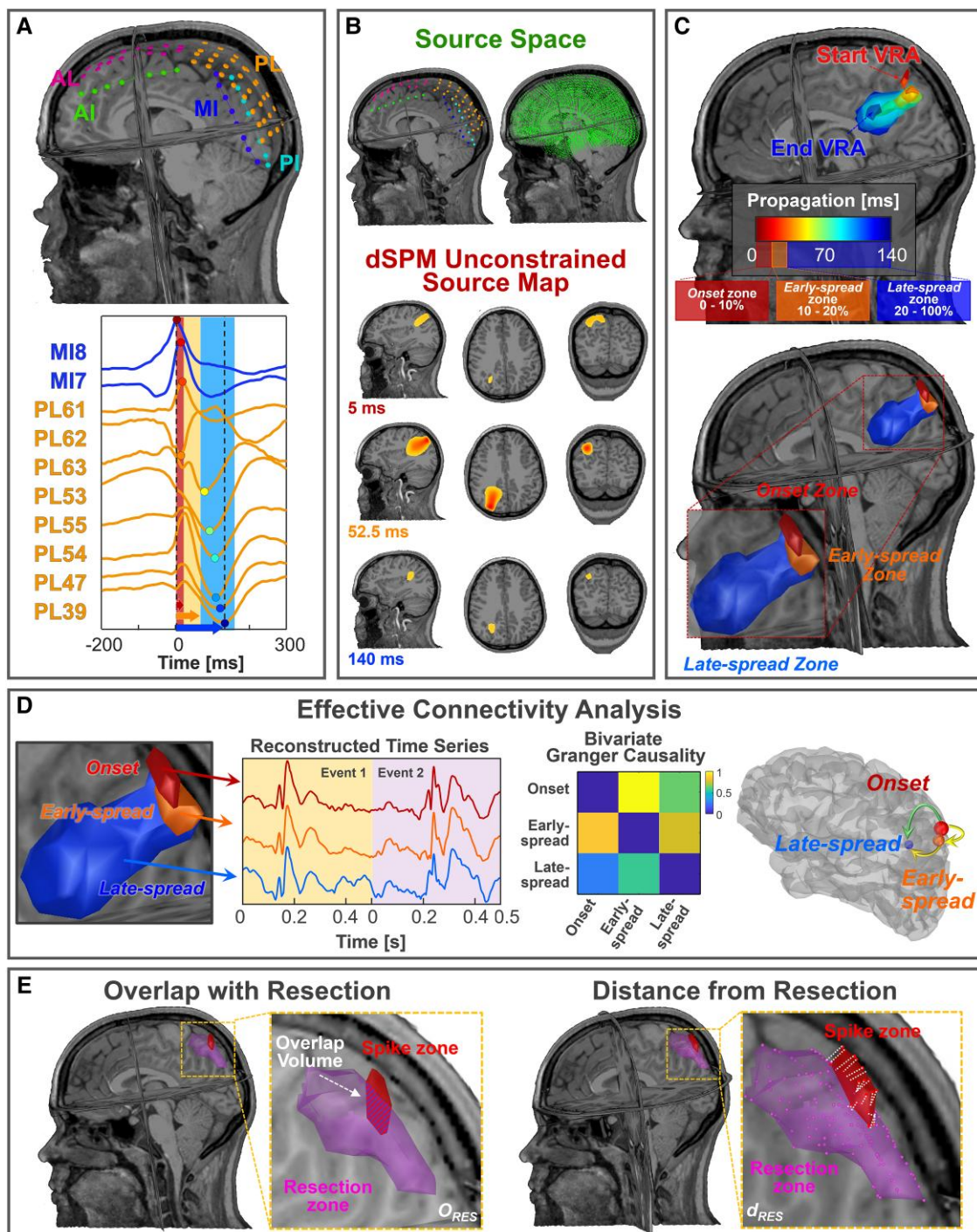
### Definition of onset, early-spread, and areas of late-spread

We defined three zones of activity in ESI spike propagation: 'onset', 'early-spread' and 'late-spread' (Fig. 1C).<sup>32,55,56</sup> We defined onset as the first 10% of the total duration of the entire phenomenon, early-spread the next 10% and late-spread the remaining 80%.<sup>44</sup> We then defined a VRA using 70% of the maximum current maps' activation as the optimal cut-off.<sup>52</sup> We estimated the spatial displacement of propagation as the sum of all distances from one VRA centre to the following one. The propagation velocity within each zone was computed by dividing the corresponding spatial displacement by its duration. We also performed ESI on each separate propagating event for each patient. We estimated the variability of spike onset localization across all propagating events by calculating the median distance of each event's spike onset from the onset, and the percentage of propagating events covered by the onset. We then compared the localization of each spike onset with the anatomical regions defined by the AAL3 atlas,<sup>57</sup> and identified predominant spike onset(s) as the regions where at least 10% of the total number of propagating events originate. Finally, we defined the isolated spike zone by localizing the most frequently occurring isolated spikes for each patient (Supplementary Fig. 1).

### Effective connectivity analysis

We computed a single time series for each zone of propagation. From each spike propagation window, we extracted the maximum across all sources for each time point. We then concatenated all reconstructed signals for each zone separately (length  $W \times 500$  ms, where  $W$  is number of propagating events for that patient; Fig. 1D). We then estimated information flow between pairs of signals through the bivariate GC algorithm<sup>58</sup> using a multivariate





**Figure 1** Methodological pipeline (data from Patient 11). (A) Locations of intracranial EEG (iEEG) leads with respect to patient's MRI (top); spike propagation on iEEG in two iEEG leads (i.e. MI, PL) (bottom). (B) Comparison between iEEG and source space spatial resolution (top); A volumetric region of activation (VRA), decomposed in the three MRI planes, estimated through dynamic statistical parametric mapping (dSPM) at three specific time points (bottom). (C) A VRA propagation created every 5 ms by averaging the activation values (above 70%) in that window (top); onset is defined as the VRA given by the union of all the VRAs within the first 10% of the duration of propagation phenomenon, early-spread is defined as the union of the VRA in the range 10–20% of the propagation and late-spread zone is defined as the VRA given by the union of all the VRAs that occur at the remaining 80% of propagation (bottom). (D) Extraction of the three time series from onset, early-spread and late-spread zones. Computation of the Granger causality (GC) matrix between these signals and corresponding graph on the cortex highlighting the information flow direction. (E) Left: evaluation of the volume percentage of ESI zones that overlaps with resection ( $O_{RES}$ ); right: localization error definition as the mean distances of the ESI zones from resection ( $d_{RES}$ ). AI = anterior interhemispheric; AL = anterior left; MI = middle interhemispheric; PI = posterior interhemispheric; PL = posterior left.

autoregressive model of 10th order. We obtained a  $3 \times 3$  non-symmetric GC matrix in which the columns and rows correspond to onset, early-spread, and late-spread; GC values were normalized

on its maximum (Fig. 1D). We employed the values in the matrix to define the information flow between pairs of regions (i.e. onset/early-spread, onset/late-spread, and early-spread/late-spread). By

subtracting the information flow from zone 1 to 2, we assessed the direction of information flow between pairs of zones (Fig. 1D), where positive or negative values indicated an information flow from zone 1 to 2 or vice versa.

### Comparison with resection and seizure onset zone

To assess the ability of each zone and the clinically-defined SOZ to approximate the EZ, we computed the percentage of overlap ( $O_{RES}$ ) and mean Euclidean distance from resection ( $d_{RES}$ ) (Fig. 1E). The  $O_{RES}$  was calculated as the ratio between the sources of each zone considered resected (i.e.  $d_{RES} \leq 10$  mm) and the total number of sources included in that zone.

To assess the clinical utility of spike propagation reconstructed through ESI, we compared the features obtained through ESI with the ones obtained at the electrodes' level. We defined iEEG spike onset as the channels that recorded the highest spikes rate within 4 ms from onset.<sup>52</sup> We also calculated the duration, spatial displacement, and velocity for each propagating event at electrodes' level.

### Prognostic value for surgical prediction

We evaluated whether each zone was able to delineate the EZ. As an indicator of outcome, we considered the  $O_{RES}$  computed for each zone and ground truth as the dichotomized patients' outcome. Using the receiver operating characteristic (ROC) curves on each zone's overlap with resection, we assessed whether removing the onset, early-spread, or late-spread and the SOZ predicted outcome. We regarded: (i) true positive (TP) as a good-outcome patient in whom the considered zone was resected; and (ii) true negative (TN) as a poor-outcome patient following missed resection of the zone under consideration. Finally, we defined false positive (FP) and false negative (FN) as poor-outcome patients with resection of the zone of interest and good-outcome patients without resection of that zone, respectively.

To reduce the variability associated with our cohort and better assess the predictive ability of each zone, we performed a leave-one-out cross-fold validation, excluding one patient for each iteration. We built a ROC curve for each iteration (based on the  $O_{RES}$ ) considering the whole sample except the  $O_{RES}$  data from one patient at the time. We then computed a mean ROC curve for each zone of interest and, by setting 50% as fixed resection percentage to discriminate between resected or non-resected zones, we extracted, the following metrics from the ROC curve: (i) sensitivity [ $SENS = TP / (TP + FN)$ ]; (ii) specificity [ $SPEC = TN / (TN + FP)$ ]; (iii) positive predictive value [ $PPV = TP / (TP + FP)$ ]; (iv) negative predictive value [ $NPV = TN / (TN + FN)$ ]; (v) accuracy [ $(TP + TN) / (TP + TN + FP + FN)$ ]; and (vi) area under the curve (AUC). We then used the whole cohort for testing if resection of a zone of interest was associated with outcome via Fisher's exact test.

### Statistical analysis

All statistical analyses were performed in MATLAB 2021a (The MathWorks, Inc.). We applied Wilcoxon signed-rank test for paired comparisons between different zones and Wilcoxon rank-sum for the non-paired comparisons between good and poor outcomes patients. False discovery rate correction was used for multiple comparisons. We calculated Spearman correlation coefficient to assess whether two variables had a rank correlation. We compared the predictive performances of all zones via the Kruskal–Wallis test. Regression analysis was performed to examine whether

pathology related to focal cortical dysplasia (FCD) or temporal lobe epilepsy localization (i.e. temporal versus extra-temporal) may influence the outcome's prediction. We assumed statistically significant results if  $P < 0.05$  and reported measures as median and interquartile range.

### Data and code availability

The data are available from the corresponding author upon request. Codes used in this work are available on GitHub at <https://github.com/matarrese/Spike-propagation-reconstruction>.

## Results

### Cohort

We report demographic and clinical information of our cohort in Table 1. We included 43 patients with a median age at surgery of 13 years (range 8.2–16 years) (Table 2). Twenty-five patients (58%) were seizure-free at least 1 year after surgery and were regarded as having a good outcome (Table 2). The volume of resection was higher for good versus poor outcome patients ( $P = 0.03$ ; Table 2), while the number of electrodes defining the SOZ was not different between groups ( $P = 0.42$ ; Table 2). We also found no differences in sex, age at surgery, age at epilepsy onset, side, pathology and follow-up between good and poor outcome patients (Table 2).

### Isolated and propagating events

We observed: (i) no difference in the percentage of isolated versus propagating events in good outcome patients [Fig. 2A; isolated: 32% (19–84%), propagating: 68% (16–81%),  $P = 0.97$ ]; (ii) a higher percentage of isolated versus propagating events in poor outcome patients [Fig. 2A; isolated: 75% (33–91%), propagating: 25% (9–67%),  $P = 0.04$ ]; and (iii) no difference in both the percentages of isolated ( $P = 0.12$ ) and propagating events ( $P = 0.12$ ) in good versus poor outcome patients. We also evaluated the rate of propagating and isolated events observing (i) a higher rate of propagating events in good versus poor outcome patients [good: 24 events/min (14–44 events/min), poor: nine events/min (4–27 events/min),  $P = 0.02$ ]; and (ii) no difference in the rate of isolated events between good versus poor outcome patients [good: 102 events/min (58–175 events/min), poor: 188 events/min (51–217 events/min),  $P = 0.86$ ].

We found no difference in spike-onset variability [Fig. 2B;  $P = 0.83$ ; 9 mm (7–23 mm) versus 13 mm (6–27 mm)] and in spike coverage percentage [ $P = 0.82$ ; 50% (31–70%) versus 43% (19–75%)] between good and poor outcome patients. We observed a median of one (one to two) propagation pattern per patient with no difference between good and poor outcome patients ( $P = 0.77$ ). We observed: (i) one predominant spike onset in 51% of our patients (Fig. 2C; 22/43, 12 good outcome); (ii) two in 26% of our patients (11/43, nine good outcome); (iii) three in 16% of our patients (7/43, four good outcome); and (iv) more than three in three poor outcome patients (7%). If there were more than one predominant spike onset, the distance between them was 10 mm (3–26 mm) in good versus 34 mm (5–43 mm) in poor outcome patients ( $P = 0.18$ ). Finally, we observed that the onset zone covered at least one predominant spike onset in 93% of patients (Fig. 2D).

### Descriptive features of propagating events

The reconstructed spike propagation had a duration of 95 ms (34–206 ms), a spatial displacement of 14 cm (7.5–22 cm), and a velocity of 0.5 m/s (0.3–0.8 m/s) with no difference between patients

Table 1 Patient demographics and clinical information

| #   | Sex | Age at surgery, years | Seizure onset, years | MRI findings                                      | Epilepsy side | Resected region | Vol. Res., cm <sup>3</sup> | iEEG (SE + DE), n | iEEG location   | Engel (f/u, years) |
|---|-----|-----------------------|----------------------|---|---------------|-----------------|----------------------------|-------------------|-----------------|--------------------|
| <b>Good surgical outcome patients (i.e. Engel ≤ 1; follow-up ≥ 1 year)</b>    |     |                       |                      |   |               |                 |                            |                   |                 |                    |
| 1   | M   | 11                    | 4                    | Normal  | R             | Fr              | 13.1                       | 80 (SE)           | Fr, T           | IA (5)             |
| 2   | F   | 7                     | 3                    | FCD (T and Ins)                                   | L             | Fr-T            | 13.7                       | 90 (DE)           | Fr, T           | IB (8)             |
| 3   | F   | 14                    | 10                   | Normal  | L             | T               | 18.7                       | 72 (SE)           | Fr, T           | IA (5)             |
| 4   | M   | 18                    | 9                    | Tumour (T)  | L             | T               | 38.5                       | 72 + 20           | Fr, T           | IC (6)             |
| 5   | F   | 16                    | 14.5                 | FCD (T)   | L             | T-Hipp.         | 23.1                       | 96 + 10           | T               | IA (8)             |
| 6   | M   | 2                     | 0.3                  | TSC (multifocal)                                  | R             | Fr              | 53.8                       | 112 (SE)          | Fr, P, IH       | IA (7)             |
| 7   | F   | 9                     | 4                    | FCD (P)   | R             | P               | 27.7                       | 80 + 20           | P, O, IH        | IB (4)             |
| 8   | F   | 18                    | 15                   | Normal  | L             | T               | 26.8                       | 88 (SE)           | Fr, T           | IA (7)             |
| 9   | M   | 15                    | 12                   | Hippocampal sclerosis (anterior T)                | L             | T               | 27.9                       | 80 (SE)           | T               | IA (2)             |
| 10  | F   | 10                    | 1                    | Low-grade neoplasm (Fr)                           | R             | Fr              | 25.2                       | 112 + 10          | Fr, P, IH       | IB (4)             |
| 11  | F   | 15                    | 6                    | FCD (mesial P)                                    | L             | Fr              | 8.2                        | 72 (SE)           | Fr, P, T        | IA (2)             |
| 12  | M   | 5                     | 0.17                 | FCD (T)   | L             | T-O             | 65.7                       | 96 (SE)           | P, T, O         | IA (1.5)           |
| 13  | M   | 12                    | 8                    | Encephalomalacia (P, superior T)                  | L             | P-T             | 13.4                       | 72 + 30           | Fr, P, T        | IC (2)             |
| 14  | F   | 3                     | 1.33                 | TSC (multifocal)                                  | L + R         | Fr (L)          | 15.3                       | 120 (SE)          | Fr, P, T        | IA (2)             |
| 15  | M   | 4                     | 1                    | FCD (Fr)  | L + R         | Fr (L)          | 28.2                       | 56 + 10           | Fr, IH          | IC (6)             |
| 16  | M   | 22                    | 5                    | FCD (CP)  | L             | Fr              | 21.9                       | 64 + 30           | Fr              | IA (3)             |
| 17  | F   | 12                    | 1.17                 | Normal (pineal cyst)                              | L             | Fr              | 29.6                       | 70 (DE)           | Fr, CG, Ins     | IA (4)             |
| 18  | M   | 13                    | 1                    | FCD (mesial T)                                    | L             | T               | 45.5                       | 92 (SE)           | Fr, T           | IA (9)             |
| 19  | M   | 10                    | 7                    | PMG (Fr, P)                                       | L             | Fr              | 60.0                       | 64 + 60           | Fr, P, T        | IB (2)             |
| 20  | M   | 4                     | 2                    | FCD (Fr)  | L + R         | Fr (R)          | 74.9                       | 128 + 10          | Fr              | IA (1.5)           |
| 21  | F   | 16                    | 3                    | Normal  | L             | Fr              | 18.0                       | 212 (DE)          | Fr, P, T        | IA (2)             |
| 22  | M   | 22                    | 2                    | FCD (lingual gyrus)                               | L             | O               | 52.1                       | 162 (DE)          | P, T, O         | IA (5)             |
| 23  | F   | 8                     | 6                    | FCD (posterior Fr)                                | L             | Insula          | 12.4                       | 164 (DE)          | Fr, P, T        | IA (4)             |
| 24  | M   | 15                    | 6                    | FCD (P)   | R             | P               | 7.6                        | 102 (DE)          | Fr, P           | IA (2)             |
| 25  | F   | 6                     | 4                    | PMG (P, T, O)                                     | L + R         | P-O (R)         | 54.1                       | 196 (DE)          | P, T, O         | IA (1)             |
| <b>Poor surgical outcome patients (i.e. Engel &gt; 1; follow-up ≥ 1 year)</b> |     |                       |                      |   |               |                 |                            |                   |                 |                    |
| 26  | M   | 19                    | 12                   | Normal  | L + R         | Fr-T-P (L)      | 47.4                       | 140 (SE)          | Fr, IH          | IIA (1)            |
| 27  | F   | 10                    | 0.3                  | Hippocampal sclerosis (mesial T, periventricular) | L             | T               | 8.5                        | 140 (DE)          | P, T, O         | IVB (6)            |
| 28  | M   | 6                     | 2                    | FCD (Fr)  | L             | Fr              | 22.7                       | 120 (SE)          | Fr, P, T        | IIIA (11)          |
| 29  | M   | 16                    | 4                    | Normal  | L             | T               | 10.9                       | 88 (SE)           | Fr, T, O        | IIB (2)            |
| 30  | M   | 16                    | 4                    | Normal (mild gliosis)                             | L             | Fr              | 5.8                        | 88 (SE)           | Fr, P, T        | IIIA (5)           |
| 31  | F   | 5                     | 0.5                  | TSC (P, O)  | L + R         | O (L)           | 78.6                       | 128 + 40          | P, O, IH        | IIIA (2)           |
| 32  | F   | 13                    | 7                    | Normal  | L + R         | Fr (R)          | 11.5                       | 112 + 10          | Fr, P, T, IH    | III (1)            |
| 33  | M   | 17                    | 1.5                  | Glioma (PO junction)                              | R             | O-P-T           | 15.8                       | 128 (SE)          | P, T, O         | IIIA (4)           |
| 34  | F   | 18                    | 4                    | FCD (Fr)  | L             | Fr              | 7.4                        | 144 + 10          | Fr, P           | IIA (1)            |
| 35  | M   | 13                    | 7                    | FCD (T)   | L             | Fr-T            | 69.9                       | 112 + 10          | Fr, T           | IIIA (6)           |
| 36  | M   | 13                    | 0                    | Infarct (MCA territory)                           | L             | Fr-T            | 47.3                       | 136 (SE)          | Fr, P, T, O     | IIA (3)            |
| 37  | M   | 18                    | 5                    | FCD (superior Fr gyr.)                            | L             | Insula          | 4.6                        | 212 (DE)          | Fr, T           | IIIA (6)           |
| 38  | F   | 22                    | 14                   | Trauma  | L + R         | F-T (R)         | 24.0                       | 120 (SE)          | Fr, P, T, O, IH | IIB (5)            |
| 39  | F   | 10                    | 8                    | FCD (Fr)  | L             | Fr-P            | 60.0                       | 96 (SE)           | Fr, P, T        | IIIA (5)           |
| 40  | F   | 7                     | 4                    | FCD (Fr operculum)                                | R             | Fr              | 8.9                        | 72 + 40           | Fr, T           | IIA (2.5)          |
| 41  | F   | 11                    | 0.75                 | Normal  | R             | T               | 25.2                       | 150 (DE)          | T, O            | III (2)            |
| 42  | M   | 10                    | 5                    | Normal  | L             | Fr              | 6.7                        | 96 + 10           | Fr, P           | III (1)            |
| 43  | F   | 15                    | 3.5                  | Hippocampal formation                             | L             | Fr              | 4.9                        | 166 (DE)          | Fr, P, T        | IIIA (4)           |

C = central; CG = cingulate gyrus; DE = depth electrodes; F = female; f/u = follow-up; FCD = focal cortical dysplasia; Fr = frontal; gyr = gyrus; iEEG = intracranial EEG; IH = intra-hemispheric; L = left; M = male; MCA = middle cerebral artery; O = occipital; P = parietal; PMG = polymicrogyria; R = right; SE = subdural electrodes; T = temporal; TSC = tuberous sclerosis complex; Vol. Res. = volume of resection.

with good and poor outcomes (Fig. 2E–G;  $P = 0.15$ ,  $P = 0.60$  and  $P = 0.48$ , respectively). We found 6/43 (14%) patients with synchronous spikes (i.e. duration <10 ms), 7/43 (16%) patients with short-latency spikes (<50 ms) and 30/43 (70%) patients with long-latency spikes (>50 ms).<sup>18</sup> We further considered only short- or long-latency spikes since synchronous spikes can be associated with volume conduction.<sup>59</sup>

At the electrode level, we found: (i) a median propagation duration of 58 ms (49–63 ms), longer in good versus poor outcomes patients [ $P = 0.03$ ; good: 62 ms (55–63 ms); poor: 54 ms (21–61 ms)]; (ii) a spatial displacement of 8.5 cm (7.0–9.8 cm) with no difference between good and poor outcome patients ( $P = 0.32$ ); and (iii) a velocity across contacts higher in poor than good outcome patients [ $P = 0.02$ , good: 1.4 m/s (1.1–1.7 m/s) versus poor: 1.9 m/s (1.6–3.0 m/s)].



Table 2 Patient demographics by outcome

| Feature                                       | Total            | Good outcome Engel I | Poor outcome Engel II–IV | P                 |
|---|------------------|----------------------|--------------------------|-------------------|
| Patients, n                                   | 43               | 25                   | 18                       | –                 |
| Male/female, n                                | 22/21            | 13/12                | 9/9                      | 1 <sup>a</sup>    |
| Age at surgery, years                         | 12 (7.3–15.8)    | 11 (6.8–15)          | 13 (9–16)                | 0.27 <sup>b</sup> |
| Age at epilepsy onset, years                  | 4 (1.4–7)        | 4 (1.3–7.3)          | 4 (1.5–7)                | 0.76 <sup>b</sup> |
| Epilepsy side                                 |                  |                      |                          |                   |
| L   | 15/12            | 8/8                  | 7/4                      | 0.91 <sup>a</sup> |
| R   | 4/4              | 3/2                  | 1/3                      |                   |
| Pathology                                     |                  |                      |                          |                   |
| Gen   | 3/5              | 2/2                  | 1/2                      |                   |
| NL  | 5/6              | 1/4                  | 4/2                      | 0.56 <sup>a</sup> |
| MCD   | 13/13            | 10/7                 | 3/6                      |                   |
| ACQ   | 4/2              | 2/1                  | 2/1                      |                   |
| iEEG type                                     |                  |                      |                          |                   |
| ECoG  | 11/6             | 5/4                  | 6/2                      | 0.86 <sup>a</sup> |
| sEEG  | 3/8              | 2/5                  | 1/3                      |                   |
| Both  | 8/7              | 6/3                  | 2/4                      |                   |
| iEEG, n                                       |                  |                      |                          |                   |
| ECoG  | 96 (86–120)      | 88 (78–100)          | 120 (92–132)             | 0.02 <sup>b</sup> |
| sEEG  | 162 (112–189)    | 162 (93–188)         | 158 (145–189)            |                   |
| Both  | 112 (101–124)    | 102(94–124)          | 122 (112–154)            |                   |
| Resection volume, cm <sup>3</sup>             | 22.7 (11.1–43.8) | 25.2 (14.9–47.2)     | 11.2 (6.7–25.2)          | 0.03 <sup>b</sup> |
| Resection percentage of total brain volume, % | 2.3 (1.1–3.8)    | 2.6 (1.8–4.4)        | 1.2 (0.7–2.9)            | 0.04 <sup>b</sup> |
| SOZ channels, n                               | 9 (5–20)         | 10 (6.75–20)         | 7 (5–22)                 | 0.42 <sup>b</sup> |
| T lobe/extra T                                | 9/34             | 6/19                 | 3/15                     | 0.71 <sup>a</sup> |
| Follow-up, years                              | 4 (2–5.8)        | 4 (2–6)              | 3.5 (2–5)                | 0.53 <sup>b</sup> |

ACQ = acquired (i.e. stroke, neoplasm or trauma); Gen = generalized; iEEG = intracranial EEG; L = left; MCD = malformation of cortical development (i.e. focal cortical dysplasia, polymicrogyria or tuberous sclerosis complex); NL = non-lesional; R = right; T = temporal.

<sup>a</sup>Fisher's exact test.

<sup>b</sup>Wilcoxon rank sum test.

For patients with good outcome, we found lower velocity in the onset compared to early- ( $P = 0.03$ ) and late-spread ( $P = 0.01$ ; Table 3). We also observed a lower volume for onset ( $P = 0.01$ ) and early-spread ( $P = 0.01$ ; Table 3) compared to late-spread.

## Information flow

Considering all patients, information flow between pairs of regions showed: (i) a predominant direction from onset to late-spread for 68% of patients; (ii) no prime direction between onset and early-spread; and (iii) a preferential direction from early- to late-spread for 73% of patients. In good outcome patients, the information flow followed a more organized pattern: information flow started from onset and then reached early- and late-spread in, respectively, 66% and 70% of cases. In 74% of good outcome patients, the preferential direction of information flow was from early- to late-spread. For poor outcome patients, the main difference occurred in the initial propagation phases, where the information flow started in 50% of patients from early-spread to other areas (Fig. 3A).

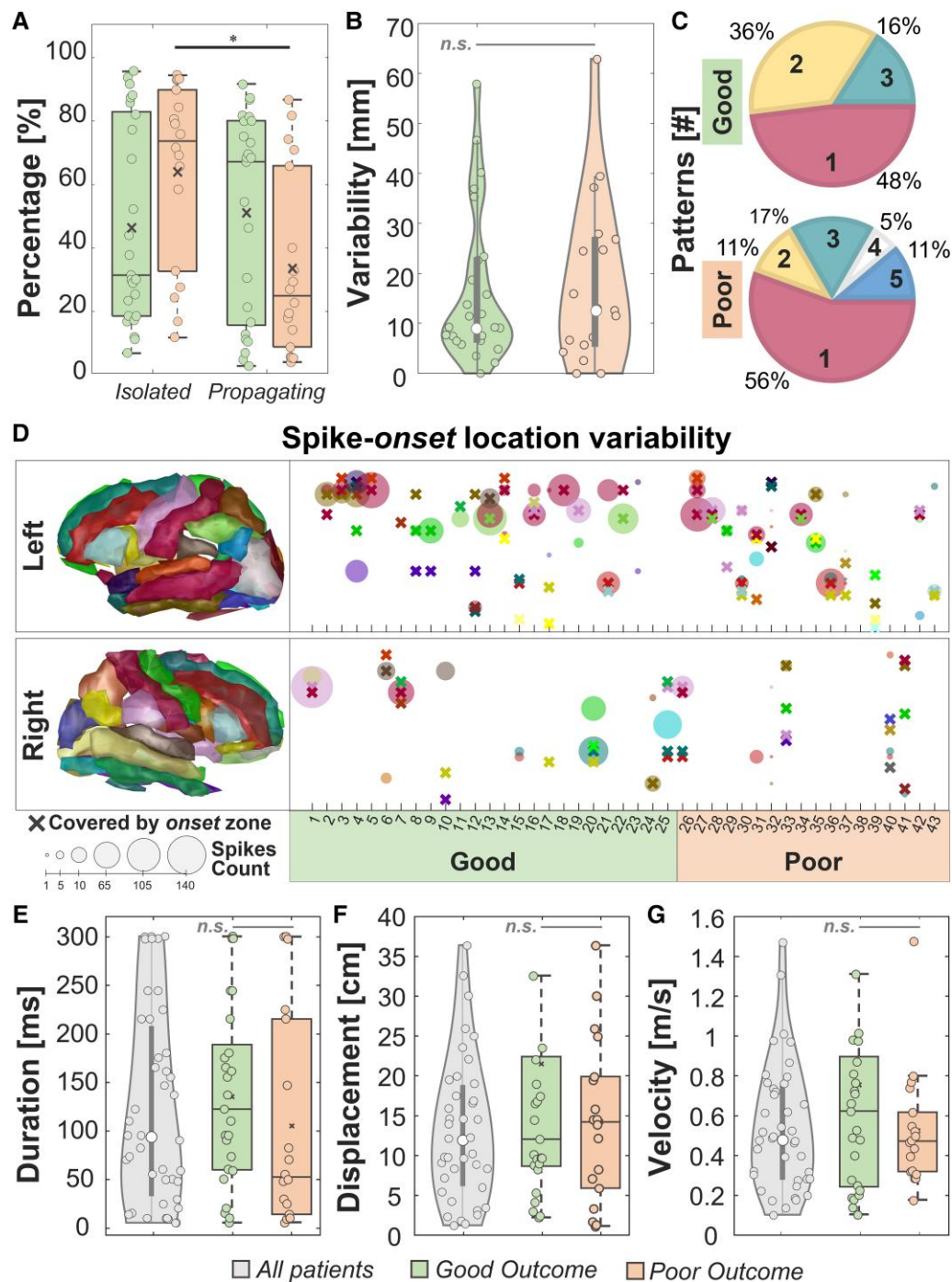
GC analysis between pairs of regions showed: (i) higher information flow from onset to early-spread [Fig. 3B;  $P = 0.006$  from Kruskal–Wallis test; 0.90 (0.71–1)], compared to information flow from late-spread to both onset [ $P = 0.004$ ; 0.31 (0.14–0.81)] and early-spread [ $P = 0.01$ ; 0.48 (0.25–0.84)], for patients with good outcome; (ii) higher information flow from onset to late-spread compared to information flow in the opposite direction for patients with good outcome [Fig. 3B;  $P = 0.02$ , 0.67 (0.35–0.87) versus 0.31 (0.14–0.81)]; (iii) higher information flow from early- to late-spread compared to information flow from late-spread to onset for patients with both good and poor outcome [Fig. 3B; good:  $P = 0.02$ , 0.73 (0.46–0.78) versus 0.31 (0.14–0.81); poor:  $P = 0.04$ , 0.88 (0.71–1) versus 0.55 (0.32–0.86)]; (iv) higher information flow from early-spread to onset compared to information flow from late-spread to onset [Fig. 3B;  $P = 0.01$ , 1

(0.78–1) versus 0.55 (0.32–0.86)] and late-spread to early-spread for patients with poor outcome [Fig. 3B;  $P = 0.01$ , 1 (0.78–1) versus 0.39 (0.18–0.90)]; (v) lower information flow from early-spread to onset in patients with good versus poor outcome [ $P = 0.01$ , 0.61 (0.42–0.99) versus 1 (0.78–1); Fig. 3B]; and (vi) lower information flow from early-spread to late-spread in patients with good versus poor outcome [ $P = 0.04$ , 0.73 (0.46–0.78) versus 0.88 (0.71–1); Fig. 3B].

## Comparison with resection and seizure onset zone

Resection percentages of all zones were higher in patients with good versus poor outcome (Fig. 3C and Table 3; onset:  $P = 0.003$ , early-spread:  $P = 0.009$ , late-spread:  $P = 0.009$ ). Onset and early-spread were closer to resection in patients with good versus poor outcome (Fig. 3D and Table 3; onset:  $P = 0.005$ ; early-spread:  $P = 0.02$ ). For patients with good outcome, the overlap of onset with resection was higher compared to both areas of spread (early-spread:  $P = 0.01$ ; late-spread:  $P = 0.002$ ). For these patients, the onset was also closer to resection compared to late-spread ( $P = 0.007$ ). We found no difference of  $O_{RES}$  and  $d_{RES}$  ( $P > 0.05$ ) between the different ESI zones in poor outcome patients. We found no difference in the  $O_{RES}$  and  $d_{RES}$  between FCD versus non-FCD patients, and between temporal versus extra-temporal patients (Supplementary Fig. 2A and B).

Comparing the onset with SOZ, we found (i) no difference of  $O_{RES}$  [ $P = 0.55$ ; 96% (40–100%) versus 76% (62–98%)] (Fig. 3E) and  $d_{RES}$  [ $P = 0.63$ ; 5 mm (4–12 mm) versus 7 mm (4–11 mm)] (Fig. 3F) for good outcome patients; (ii) a lower  $O_{RES}$  for onset in patients with poor outcome [ $P = 0.01$ ; 13% (0–71%) versus 65% (59–85%)] (Fig. 3E); and (iii) a higher  $d_{RES}$  for the onset in patients with poor outcome [ $P = 0.04$ ; 22 (9–29 mm) versus 10 (5–18 mm)] (Fig. 3F). Onset and early-spread were included in the SOZ in 61% of patients with good outcome, while the late-spread in 43% of patients. In poor outcome patients,



**Figure 2 Descriptive features.** (A) Percentages of isolated and propagating events in good versus poor outcome patients. (B) Variability of spike onset(s) from the onset zone. (C) Predominant spike onset(s) number for good versus poor outcome patients. (D) Spike onset location variability per patient, separated per right and left hemisphere. Each cross represents an anatomical area covered by the onset zone while the circle is an area covered by a predominant spike onset. The dimension of the circle represents the number of events originating from that area. (E) Duration, (F) spatial displacement and (G) velocity of spike propagation for all patients. In all the panels, the black line identifies a comparison with  $P < 0.05$  via paired sign-rank test and the grey line identifies a non-significant (n.s.) rank-sum test. In the box plots, the cross identifies the mean value, the line is the median, the lower and upper edges are, respectively, the 25th and 75th percentiles, while the whiskers range from the minimum to the maximum values (disregarding the outliers).

onset was included in the SOZ in 36% of our cohort while the early-spread and late-spread in 29% and 14%, respectively.

Finally, we compared the onset with the iEEG spike onset. We found: (i) a higher  $O_{RES}$  for the onset compared with the iEEG spike onset [Fig 3G;  $P = 0.04$ ; 96% (40–100%)] versus 43% (25–79%)] and a lower  $d_{RES}$  for the

onset compared with the iEEG spike onset [Fig 3H;  $P = 0.03$ ; 5 mm (4–12 mm) versus 16 mm (6–223 mm)] for patients with good outcome, and (ii) no difference of  $O_{RES}$  [ $P = 0.79$ ; 13% (0–71%) versus 25% (11–61%)] and  $d_{RES}$  [ $P = 0.58$ ; 22 mm (9–29 mm) versus 19 mm (13–26 mm)] for poor outcome patients.



Table 3 Characteristics of ESI zones by outcome

| Feature  | Zone  |                  |                  | P                |                 |              |         |
|--|-------|------------------|------------------|------------------|-----------------|--------------|---------|
|  | Onset | ES               | LS               | Onset versus ES  | Onset versus LS | ES versus LS |         |
| <b>Good outcome patients (n = 23)—poor outcome patients (n = 14)</b> |       |                  |                  |                  |                 |              |         |
| Time duration, ms  | Good  | 25 (16–30)       | 25 (15–30)       | 160 (106–180)    | 0.47            | <0.001*      | <0.001* |
|  | Poor  | 26 (14–30)       | 30 (20–49)       | 131 (73–175)     | 0.64            | 0.005*       | –       |
|  | P     | 0.74             | 0.24             | 0.39             | –               | –            | 0.005*  |
| Spatial displacement, cm   | Good  | 0.6 (0.25–1)     | 0.7 (0.3–1.4)    | 6.4 (3.6–13.5)   | 0.12            | <0.001*      | <0.001* |
|  | Poor  | 0.5 (0.25–0.7)   | 0.3 (0.3–0.5)    | 3.2 (0.8–6.4)    | 0.1             | 0.02*        | –       |
|  | P     | 0.7              | 0.05             | 0.02†            | –               | –            | <0.001* |
| Velocity, m/s  | Good  | 0.25 (0.12–0.59) | 0.46 (0.16–0.66) | 0.53 (0.26–1.15) | 0.03*           | 0.01*        | 0.28    |
|  | Poor  | 0.22 (0.09–0.62) | 0.14 (0.09–0.26) | 0.36 (0.14–0.87) | 0.13            | 0.89         | 0.13    |
|  | P     | 0.81             | 0.047†           | 0.22             | –               | –            | –       |
| Volume, cm <sup>3</sup>  | Good  | 3.5 (0.7–6.0)    | 7.2 (1.3–15.3)   | 14.1 (2.6–63.9)  | 0.08            | 0.01*        | 0.01*   |
|  | Poor  | 7.2 (1.2–28.7)   | 1.2 (0.2–20.8)   | 12.5 (3.2–24.1)  | 0.65            | 0.57         | 0.18    |
|  | P     | 0.19             | 0.28             | 0.79             | –               | –            | –       |
| Sources active, %  | Good  | 0.56 (0.21–1.04) | 0.84 (0.23–1.41) | 1.39 (0.49–2.63) | 0.07            | <0.001*      | 0.005*  |
|  | Poor  | 0.99 (0.17–2.09) | 0.18 (0.08–1.3)  | 0.92 (0.33–1.97) | 0.65            | 0.38         | 0.17    |
|  | P     | 0.63             | 0.15             | 0.58             | –               | –            | –       |
| Overlap with resection, %  | Good  | 96 (40–100)      | 86 (34–100)      | 59 (12–100)      | 0.01*           | 0.002*       | 0.09    |
|  | Poor  | 13 (0–71)        | 14 (0–71)        | 7 (0–61)         | 0.47            | 0.21         | 0.37    |
|  | P     | 0.003†           | 0.009†           | 0.009*           | –               | –            | –       |
| Distance from resection, mm  | Good  | 4.6 (3.7–11.7)   | 6.2 (3.7–16.1)   | 8.7 (4.2–27.2)   | 0.05            | 0.007*       | 0.09    |
|  | Poor  | 21.6 (9.9–28.6)  | 22.8 (9–30)      | 23 (9.5–32.4)    | 0.43            | 0.09         | 0.27    |
|  | P     | 0.005†           | 0.02†            | 0.06             | –               | –            | –       |
| Overlap with SOZ, %  | Good  | 76 (21–100)      | 72 (6–98)        | 33 (8–88)        | 0.33            | 0.01*        | 0.04*   |
|  | Poor  | 3 (0–67)         | 3 (0–67)         | 1 (0–28)         | 1               | 0.04*        | 0.04*   |
|  | P     | 0.02†            | 0.06             | 0.005†           | –               | –            | –       |
| Distance from SOZ, mm  | Good  | 6.5 (2.3–18)     | 7 (2.9–25.5)     | 14.7 (5.8–22.2)  | 0.16            | 0.01*        | 0.08    |
|  | Poor  | 23.7 (8.6–32.2)  | 31.4 (8.6–35.4)  | 31.8 (15.8–37)   | 0.1             | 0.13         | 0.41    |
|  | P     | 0.03†            | 0.05             | 0.03†            | –               | –            | –       |

ES = early-spread; LS = late-spread.

\*Comparison with  $P < 0.05$  via paired sign-rank test.

†Significant ( $P < 0.05$ ) non-paired rank-sum test.

To highlight the relationship of onset with the EZ, we mapped the spatiotemporal propagation of spikes for two patients: one with good and one with poor outcome (Fig. 4). In the good outcome patient, the onset was overlapped to resection while areas of spread were only partially included in the resection. For this patient, information flow had a predominant direction from onset to early-spread. Contrarily, in the poor outcome patient, the onset was not overlapping with resection, while information flow had an opposite predominant direction: from early-spread to onset.

### Prognostic value

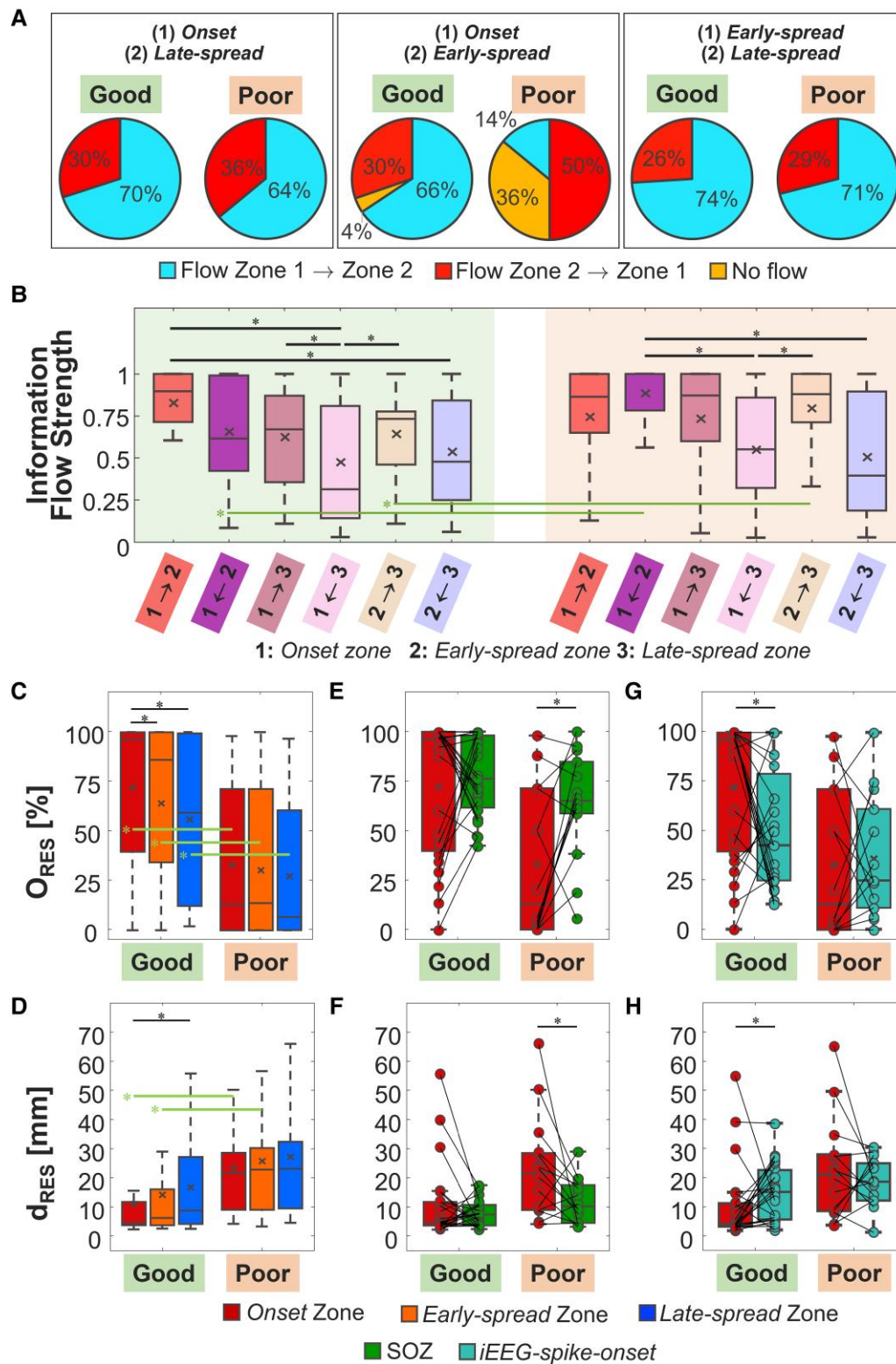
Figure 5 reports the prognostic value of resecting the onset, early-spread, late-spread, clinically-defined SOZ, and iEEG spike onset. From the ROC curves analysis (Fig. 5A), we observed the highest prediction performance for the onset, since it had a PPV of 79%, an NPV of 56% and an accuracy of 69% and was the only biomarker able to predict outcome ( $P = 0.04$ ; Fig. 5B). The predictive performance of the rest of the zones did not reach significance ( $P > 0.05$ ; Fig. 5B). Regression analysis showed that adding the EZ localization (temporal versus extratemporal) and underlying pathology (FCD versus non-FCD) along with the onset  $O_{RES}$  did not influence the outcome prediction (Supplementary Fig. 2C and D).

From the leave-one-out cross-validation, we found that the clinically-defined SOZ showed the highest sensitivity [0.86 (0.86–0.87),  $P < 0.001$ ; Fig. 5C] but the lowest specificity [0.21 (0.21–0.23),  $P < 0.001$ ; Fig. 5D] compared to all other biomarkers. The onset

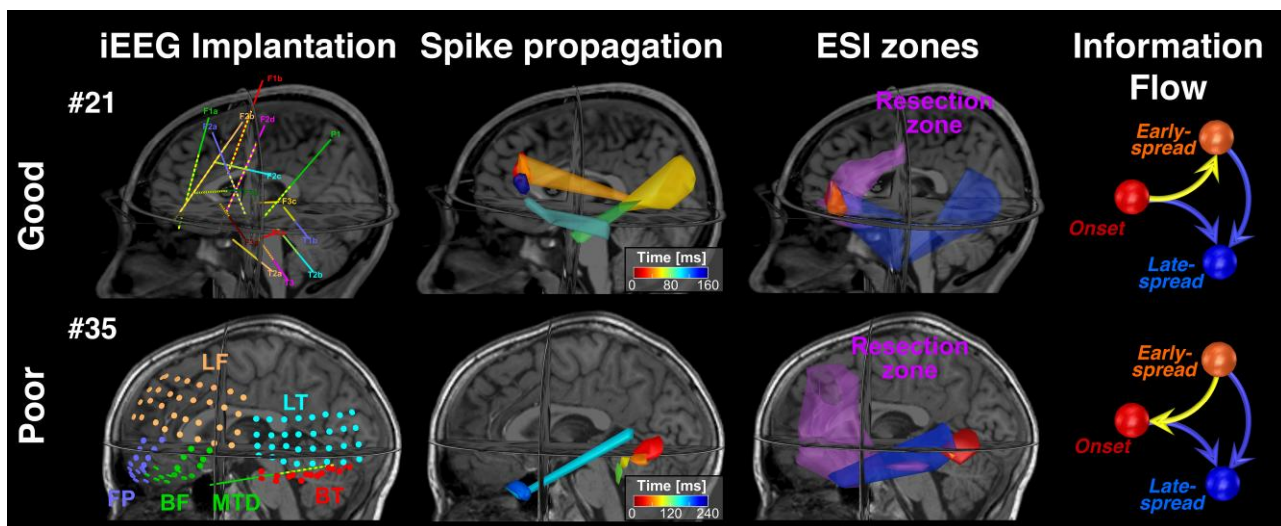
showed the highest accuracy [0.67 (0.67–0.69),  $P < 0.001$ ; Fig. 5E], while the iEEG spike onset showed the lowest accuracy [0.53 (0.53–0.56),  $P < 0.001$ ; Fig. 5E]. The onset showed the highest PPV and NPV [PPV: 0.79 (0.78–0.79); NPV: 0.56 (0.53–0.56); Fig. 5F and G], and the best AUC [0.79 (0.79–0.81),  $P < 0.001$ ; Fig. 5H]. Results for prediction performances separately for ECoG and sEEG were provided in Supplementary Fig. 3.

### Discussion

By mapping the spatiotemporal propagation of spikes through ESI performed on iEEG and estimating the effective connectivity among involved brain regions, we show that information flows outwards from areas of onset to areas of spread following a hierarchical epileptogenic organization: areas where spikes are initiated (i.e. onset) are more epileptogenic compared to areas of spread (i.e. early spread and late spread). Thus, resection of onset, but not areas of spread, disrupts the epileptogenic functional network predicting outcome and rendering patients with DRE seizure-free. This notion derives from our main findings showing that: (i) interictal epileptiform activity has a predominant directionality in information flow from onset to areas of spread only for patients with good outcome; (ii) overlap with resection is higher for patients with good outcome for onset compared to areas of spread; (iii) onset shows more overlap and lower distance from resection in patients with good versus poor outcome; (iv) resection of onset predicts outcome; and (v)



**Figure 3 ESI and information flow findings.** (A) Percentages of the principal direction of information flow considering pairs of regions for all patients and for good versus poor outcome group (left: onset/late-spread, middle: onset/early-spread, right: early/late-spread). (B) Information flow values between pair of regions [from the Granger causality (GC) matrix]. (C) Overlap with resection in percentage for the three spike zones ( $O_{RES}$ ). (D) Distance from resection ( $d_{RES}$ ) in mm for the three spike zones. (E) Comparison of the  $O_{RES}$  for the onset zone and the clinically-defined seizure onset zone (SOZ). (F) Comparison of the  $d_{RES}$  for the onset zone and the clinically-defined SOZ. (G) Comparison of the  $O_{RES}$  for the onset zone and the intracranial EEG (iEEG) spike onset. (H) Comparison of the  $d_{RES}$  for the onset zone and the iEEG spike onset. In all panels, the black line identifies a comparison with  $P < 0.05$  via paired sign-rank test while the green line is for a significant non-paired rank-sum test. In the box plots, the cross identifies the mean value, the line is the median, the lower and upper edges are, respectively, the 25th and 75th percentiles, while the whiskers range from the minimum to the maximum values (disregarding the outliers).



**Figure 4** ESI spike propagation and information flow examples for good and poor outcome patients. In the *first* column, we report the positions of the intracranial EEG (iEEG) contact on patient's MRI. The *second* column contains a simplified version of the spike propagation in source space. The volumetric regions of activation (VRAs) are colour map coloured and each colour is a specific time sample (for sake of clarity we do not report all VRAs in propagation). In the *third* column, we report the three zones defined splitting the propagation (onset in red; early-spread in orange and late-spread in blue) and the resection volume (purple). Finally, in the *fourth* column is reported the Information Flow graph [from the Granger causality (GC) matrix made on the three regions of interest (ROIs)], where the arrow direction indicates that the information flow is towards that zone. ESI = electrical source imaging.

resection of areas of spread (or the clinically-defined SOZ) do not predict outcome. Our study links two separate bodies of literature on the propagation of epileptiform activity and effective connectivity providing novel insights regarding the pathophysiological mechanism of propagating epileptiform activity within the framework of epilepsy as a network disorder. More importantly, it highlights the clinical value of onset as an interictal biomarker that may enhance surgical planning in children suffering from DRE.

### Quantifying features of spatiotemporal spike propagation through ESI

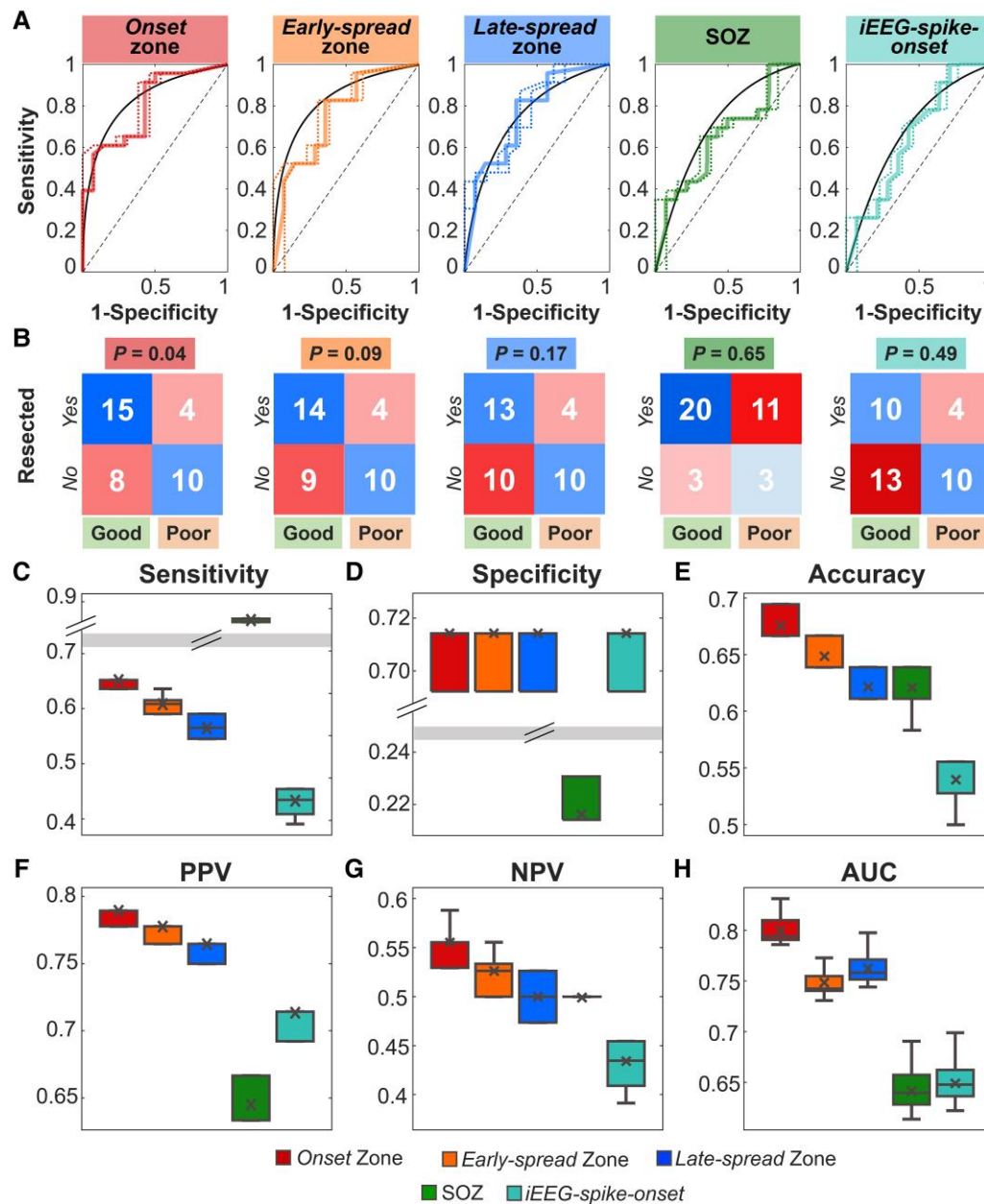
Propagating activity in epilepsy is conventionally related to ictal interpretation on iEEG recordings.<sup>60,61</sup> Recent studies extended the concept of propagation to interictal activity, such as spikes<sup>18,21,62,63</sup> and ripples.<sup>48,52,64</sup> Yet, our understanding of these mechanisms is still elusive. Here, we evaluated the mechanism of spike propagation by estimating spatiotemporal features [i.e. predominant spike onset(s), spike-onset variability, propagation duration, velocity, and spatial displacement] through ESI performed on iEEG. We speculated that ESI performed on iEEG may overcome the limited spatial resolution of iEEG leading to proper interpretation of the propagation phenomenon.<sup>24</sup> Our study builds on existing literature by showing that: (i) good outcome patients have a higher rate of propagating events compared to poor outcome; (ii) poor outcome patients have more isolated than propagating spikes; (iii) spike propagations have a median of one predominant spike onset; (iv) variability of spike onset(s) localization is  $\sim 10$  mm from the onset zone; (v) the onset zone covers at least one predominant spike onset; (vi) spikes propagate with a velocity of 0.5 m/s; (vii) propagation is initiated focally and propagates later quickly to areas of spread (e.g. lower velocity at onset versus early- and late-spread); (viii) propagation duration is  $\sim 95$  ms; and (ix) spatial propagation displacement is  $\sim 14$  cm.

Our findings indicate that propagating events were possibly not entirely sampled in patients with poor outcome; implanted

electrodes may have left uncovered areas which initiated the predominant spike onset. This may explain the higher percentage of isolated versus propagating spikes in patients with poor outcome (Fig. 2A). When propagating events were captured by the implanted electrodes, their onset(s) showed a low variability ( $\sim 10$  mm) in the localization from the onset zone (Fig. 2B). Most patients in our cohort showed either one predominant spike onset, or if more than one, the spike onsets were far apart  $\sim 10$  mm (in good outcome patients) belonging possibly to the same gyrus. Thus, the estimated onset zone represented a reliable estimator of the predominant spike onset(s) in our cohort.

Experimental models at the cellular level had showed that epileptic activity can propagate with a velocity of  $\sim 0.1$  m/s.<sup>65</sup> Electrophysiological studies in epilepsy patients with implanted macroelectrodes have showed a velocity of  $>1$  m/s.<sup>18,19,52</sup> The velocity observed here (0.5 m/s) is within the range of previously reported values; this can be attributed to our ESI approach that provides a more realistic quantification of velocity bridging findings derived from recordings at the micro- (cellular) and macro-level (macroelectrodes). Previous studies<sup>19,21</sup> demonstrated that areas where spikes originate are within the EZ and act as 'pacemakers' while areas where spikes propagate are less epileptogenic. Our finding may corroborate this concept since we observed a slower velocity in the first phase of propagation, which was then increased during later stages. The initial slow phase at onset may serve as a recruiting mechanism of a sufficient neuronal population for triggering the initiation of propagation, acting as 'generator'. After this initial neural recruitment within onset, neural activity may be transmitted through fiber paths with an increasing velocity. Former iEEG studies on spike propagation reported findings related to duration and spatial distributions along the cortex, pointing out how spikes activity is an intricate phenomenon involving broad cortical areas as well as deep brain structures.<sup>18,19</sup> A duration of up to 220 ms was previously reported for spike propagation from deep structures and the neocortex in human iEEG.<sup>18</sup> Similarly, we found here a duration ranging from  $\sim 35$  up to  $\sim 210$  ms.





**Figure 5 Outcome prediction results.** (A) From left to right: ROC curves and their confidence intervals for  $O_{RES}$  of the onset zone, early-spread zone, late-spread zone, clinically-defined SOZ and iEEG spike onset as predictor of the post-surgical outcome. (B) Confusion matrices for each region of interest (ROI) obtained on the whole cohort, setting 50% as best threshold for evaluating the post-surgical outcome. (C) Sensitivity, (D) specificity, (E) accuracy, (F) positive predictive value (PPV), (G) negative predictive value (NPV) and (H) area under the curve (AUC) leave-one-out cross validated measures evaluated for each ROI. In A, the black line is the convex hull of the mean ROC curve (i.e. continuous coloured line), while the dashed lines are the superior and inferior ranges. In the box plots, the cross identifies the mean value, the line is the median, the lower and upper edges are, respectively, the 25th and 75th percentiles, while the whiskers range from the minimum to the maximum values (disregarding the outliers).

### Information flows outwards from onset to areas of spread

Epilepsy is currently thought to be a dysregulation of the normal brain network behaviour. Deeper understanding of this defect may lead to a cure for managing and preventing seizures.<sup>26,66</sup> Effective connectivity is the most efficient method for studying this phenomenon because it can identify nodes driving information flow from those receiving that flow.<sup>67</sup> Previous studies from our group and others determined whether interictal iEEG could produce GC maps that delineate the EZ and predict outcome.<sup>28,68–72</sup> Nevertheless, the available findings are

contradictory: most studies report that iEEG electrodes with the highest outflow connectivity are more likely correlated with the epileptic networks and the SOZ,<sup>28,68</sup> while others report the opposite effect (i.e. highest inflow connectivity).<sup>29,73–75</sup> Previous literature also investigated the possibility to enhance the EZ delineation by combining effective connectivity with ESI in non-invasive EEG.<sup>72,76</sup> Here, we found that information flow of spikes has a predominant directionality from onset to areas of spread for patients with good outcome. Contrarily, in patients with poor outcome, information flow did not show a preferential direction during the initial phases of propagation.

Yet, lower information flow was observed from early-spread to onset and late-spread for patients with good versus poor outcome. Our findings support a hierarchical organization of the propagation zones (i.e. epileptogenicity of brain tissue decreases with spread), which coincides with an information outflow from onset to areas of spread. This organization was preserved in patients with good outcome,<sup>15</sup> as suggested by the higher outflow percentage from onset towards early-spread (66%) compared to patients with poor outcome (14%). This organization was not preserved in poor outcome patients possibly due to: (i) partial coverage of the EZ by the implanted electrodes, which missed the actual spike onset; (ii) less consistent and variable propagation patterns; or (iii) significantly fewer propagating spikes, which affected the length of reconstructed time series altering the values of GC.

### Spike-onset is better approximator of the epileptogenic zone compared to spike-spread and seizure onset zone

Despite recent technological advances in neuroimaging, the delineation of the EZ remains ambiguous.<sup>11</sup> Currently, long-term iEEG is the gold standard method for recording seizures and tracing the SOZ. Nevertheless, there is a consensus in considering the regions where interictal epileptic activity arise as more epileptic than the regions where epileptic activities spread over time.<sup>52,77</sup> Thus, we hypothesized that spike onset (identified via ESI) is more epileptogenic than areas where spikes propagate and the clinically-defined SOZ. We further hypothesized that onset is superior in localizing the EZ than the iEEG spike onset identified at the electrodes level. Here, in good outcome patients, onset areas showed: (i) higher overlap with resection than early or late spread; and (ii) higher overlap with resection compared to the clinically-defined SOZ and the iEEG spike onset. Contrarily, in poor outcome patients, onset was more remote and less overlapping with resection compared to the clinically-defined SOZ.

To our knowledge, only few studies have investigated the clinical relevance of spike propagation.<sup>20,21</sup> Hufnagel et al.<sup>20</sup> found that onset and seizure onset share common generators; surgical removal of the areas where those propagate is not necessary to achieve seizure freedom. Our results further support this notion, since in patients with good outcome, onset was overlapped with resection more than areas of spread (onset: 96% versus early spread: 86% versus late spread: 59%, Fig. 3C). Yet, in poor outcome patients, where the EZ was possibly missed (or its resection was incomplete), onset was not removed in 12 of 14 patients, resulting in lower overlap with resection and higher distance from it. Our findings also suggest a superiority of onset (defined via ESI) with respect to zones conventionally used in clinical practice (i.e. clinically-defined SOZ and irritative zone). The iEEG spike onset had an overlap with resection reduced by half in patients with good outcomes compared with the onset via ESI (43% versus 96%; Fig. 3G), indicating lower specificity to the EZ for iEEG spike onset. Yet, the SOZ was highly sensitive to the EZ, i.e. it was able to identify the EZ in patients with good outcome, but its resection did not manage the seizures in poor outcome patients, leading to an ineffective surgery. On the other hand, onset identified another portion of tissue far from resection that was not included in the SOZ (Fig. 3D–F) as possible generator of the epileptic activity. Resection (or deactivation) of this generator may have rendered the patient seizure-free.

### Resection of spike-onset, but not spike-spread neither seizure onset zone, predicts outcome

The most important clinical finding is that resection of onset predicts outcome. Contrary, resecting areas of spread, the clinically-

defined SOZ, or the iEEG spike onset did not predict outcome (Fig. 5). We found no difference in the SOZ removal between patients with good and poor outcome.<sup>78</sup> This finding highlights the notion that poor outcome is not always the result of unsuccessful resection of iEEG contacts where SOZ locates. Moreover, we found no overlap between onset and the clinically-defined SOZ in 64% of patients with poor outcome; in these patients, the onset was not resected. Only four patients in our cohort with resected onset had poor outcome. Moreover, specific EZ localizations or pathologies (e.g. temporal lobe epilepsies or FCD) had no effect on the onset ability to predict outcome in our cohort (Supplementary Fig. 2). This discrepancy between previous findings<sup>72,79</sup> and our study may be due to the different ages in cohorts (i.e. adults versus paediatric). Our findings highlight the clinical utility of onset as a precise biomarker of the EZ for evaluating the portion of brain tissue to resect.

### Limitations and future perspective

Our study examines a single center heterogeneous cohort of children with DRE having different pathologies. Future larger multicenter studies would allow the classification of patients into homogeneous subgroups investigating whether variable aetiology or pathology might alter the information flow within the epileptogenic network. Owing to the limited spatial resolution of iEEG, we were unable to inquire the propagation in the entire brain. Future studies using full coverage neuroimaging techniques, such as magnetoencephalography or high-density EEG, may address this issue. Finally, our study focuses exclusively on propagating interictal epileptiform discharges without examining propagation of ictal phenomena.

### Conclusions

By mapping the spatiotemporal propagation of interictal spikes through ESI performed on iEEG and estimating the effective connectivity among involved brain regions, we show that information flows outwards from areas of onset to areas of spread following a hierarchical epileptogenic organization: areas where spikes are initiated are more epileptogenic compared to areas of spread. Thus, resection of onset, but not areas of spread, disrupts the epileptogenic functional network predicting outcome and rendering patients with DRE seizure-free. Our study links two separate bodies of literature on the epileptiform activity propagation and FC providing novel insights regarding the pathophysiological mechanism of propagating epileptiform activity within the framework of epilepsy as a network disorder. More importantly, it highlights the clinical value of onset as an interictal biomarker of epilepsy. Such a biomarker may improve the interpretation of iEEG readings, reduce the need for prolonged monitoring, and enhance surgical planning in children suffering from DRE.

### Acknowledgements

M.A.G.M., A.L. and S.F. acknowledge the support of the National Group for Mathematical Physics (GNFM-IndAM).

### Funding

This work was supported by the National Institute of Neurological Disorders & Stroke (RO1NS104116-01A1, PI: Christos Papadelis).

## Competing interests

The authors report no competing interests.

## Supplementary material

Supplementary material is available at Brain online.

## References

- Schmidt D. Drug treatment of epilepsy: Options and limitations. *Epilepsy Behav.* 2009;15:56–65.
- Ryvlin P, Cross JH, Rheims S. Epilepsy surgery in children and adults. *Lancet Neurol.* 2014;13:1114–1126.
- Skirrow C, Cross JH, Cormack F, Harkness W, Vargha-Khadem F, Baldeweg T. Long-term intellectual outcome after temporal lobe surgery in childhood. *Neurology.* 2011;76:1330–1337.
- Guan J, Karsy M, Ducis K, Bollo RJ. Surgical strategies for pediatric epilepsy. *Transl Pediatr.* 2016;5:55–66.
- Lüders HO, Najm I, Nair D, Widdess-Walsh P, Bingman W. The epileptogenic zone: General principles. *Epileptic Disord.* 2006;8(Suppl):S1–S9.
- Rosenow F, Lüders H. Presurgical evaluation of epilepsy. *Brain.* 2001;124:1683–1700.
- Bauer S, Rosenow F. The irritative zone and seizure onset zone in subdural EEG. In: *Invasive studies of the human epileptic brain.* Oxford University Press; 2018:98–105.
- Kim DW, Kim HK, Lee SK, Chu K, Chung CK. Extent of neocortical resection and surgical outcome of epilepsy: Intracranial EEG analysis. *Epilepsia.* 2010;51:1010–1017.
- Bulacio JC, Jehi L, Wong C, et al. Long-term seizure outcome after resective surgery in patients evaluated with intracranial electrodes. *Epilepsia.* 2012;53:1722–1730.
- Widjaja E, Li B, Schinkel CD, et al. Cost-effectiveness of pediatric epilepsy surgery compared to medical treatment in children with intractable epilepsy. *Epilepsy Res.* 2011;94:61–68.
- Papadelis C, Perry MS. Localizing the epileptogenic zone with novel biomarkers. *Semin Pediatr Neurol.* 2021;39:100919.
- Lee CH, Lim SN, Lien F, Wu T. Duration of electroencephalographic recordings in patients with epilepsy. *Seizure.* 2013;22:438–442.
- Frauscher B, Bartolomei F, Kobayashi K, et al. High-frequency oscillations: The state of clinical research. *Epilepsia.* 2017;58:1316–1329.
- Mäliia MD, Meritam P, Scherg M, et al. Epileptiform discharge propagation: Analyzing spikes from the onset to the peak. *Clin Neurophysiol.* 2016;127:2127–2133.
- Tomlinson SB, Bermudez C, Conley C, Brown MW, Porter BE, Marsh ED. Spatiotemporal mapping of interictal spike propagation: A novel methodology applied to pediatric intracranial EEG recordings. *Front Neurol.* 2016;7:229.
- Emerson RG, Turner CA, Pedley TA, Walczak TS, Forgiione M. Propagation patterns of temporal spikes. *Electroencephalogr Clin Neurophysiol.* 1995;94:338–348.
- Khoo HM, von Ellenrieder N, Zazubovits N, He D, Dubeau F, Gotman J. The spike onset zone: The region where epileptic spikes start and from where they propagate. *Neurology.* 2018;91:e666–e674.
- Alarcon G, Guy CN, Binnie CD, Walker SR, Elwes RDC, Polkey CE. Intracerebral propagation of interictal activity in partial epilepsy: Implications for source localization. *J Neurol Neurosurg Psychiatry.* 1994;57:435–449.
- Baumgartner C, Lindinger G, Ebner A, et al. Propagation of interictal epileptic activity in temporal lobe epilepsy. *Neurology.* 1995;45:118–122.
- Hufnagel A, Dümpelmann M, Zentner J, Schijns O, Elger CE. Clinical relevance of quantified intracranial interictal spike activity in presurgical evaluation of epilepsy. *Epilepsia.* 2000;41:467–478.
- Alarcon G, Garcia Seoane JJ, Binnie CD, et al. Origin and propagation of interictal discharges in the acute electrocorticogram. Implications for pathophysiology and surgical treatment of temporal lobe epilepsy. *Brain.* 1997;120(Pt 12):2259–2282.
- Ramantani G, Kadish NE, Strobl K, et al. Seizure and cognitive outcomes of epilepsy surgery in infancy and early childhood. *Eur J Paediatr Neurol.* 2013;17:498–506.
- Tamilia E, Alhilani M, Tanaka N, et al. Assessing the localization accuracy and clinical utility of electric and magnetic source imaging in children with epilepsy. *Clin Neurophysiol.* 2019;130:491–504.
- Alhilani M, Tamilia E, Ricci L, et al. Ictal and interictal source imaging on intracranial EEG predicts epilepsy surgery outcome in children with focal cortical dysplasia. *Clin Neurophysiol.* 2020;131:734–743.
- Nakasato N, Levesque MF, Barth DS, Baumgartner C, Rogers RL, Sutherling WW. Comparisons of MEG, EEG, and EcoG source localization in neocortical partial epilepsy in humans. *Electroencephalogr Clin Neurophysiol.* 1994;91:171–178.
- Van Diessen E, Diederer SJH, Braun KPJ, Jansen FE, Stam CJ. Functional and structural brain networks in epilepsy: What have we learned? *Epilepsia.* 2013;54:1855–1865.
- Kramer MA, Cash SS, Angelica MD, Fong Y. Epilepsy as a disorder of cortical network organization. *Neuroscientist.* 2012;18:360–372.
- Park EH, Madsen JR. Granger causality analysis of interictal iEEG predicts seizure focus and ultimate resection. *Neurosurgery.* 2018;82:99–109.
- Narasimhan S, Kundassery KB, Gupta K, et al. Seizure-onset regions demonstrate high inward directed connectivity during resting-state: An SEEG study in focal epilepsy. *Epilepsia.* 2020;61:2534–2544.
- Korzeniewska A, Cervenka MC, Jouny CC, et al. Ictal propagation of high frequency activity is recapitulated in interictal recordings: Effective connectivity of epileptogenic networks recorded with intracranial EEG. *Neuroimage.* 2014;101:96–113.
- Wilke C, Worrell G, He B. Graph analysis of epileptogenic networks in human partial epilepsy. *Epilepsia.* 2011;52:84–93.
- Lagarde S, Roehri N, Lambert I, et al. Interictal stereotactic-EEG functional connectivity in refractory focal epilepsies. *Brain.* 2018;141:2966–2980.
- Shah P, Bernabei JM, Kini LG, et al. High interictal connectivity within the resection zone is associated with favorable post-surgical outcomes in focal epilepsy patients. *Neuroimage Clin.* 2019;23:101908.
- Antony AR, Alexopoulos AV, González-Martínez JA, et al. Functional connectivity estimated from intracranial EEG predicts surgical outcome in intractable temporal lobe epilepsy. *PLoS One.* 2013;8:e77916.
- Englot DJ, Hinkley LB, Kort NS, et al. Global and regional functional connectivity maps of neural oscillations in focal epilepsy. *Brain.* 2015;138(Pt 8):2249–2262.
- Van Dellen E, Douw L, Hillebrand A, et al. Epilepsy surgery outcome and functional network alterations in longitudinal MEG: A minimum spanning tree analysis. *Neuroimage.* 2014;86:354–363.
- Friston KJ. Functional and effective connectivity: A review. *Brain Connect.* 2011;1:13–36.
- Sporns O. Structure and function of complex brain networks. *Dialogues Clin Neurosci.* 2013;15:247–262.
- Kaminski MJ, Blinowska KJ. A new method of the description of the information flow in the brain structures. *Biol Cybern.* 1991;65:203–210.



40. Sameshima K, Antonio Baccalá L. Using partial directed coherence to describe neuronal ensemble interactions. *J Neurosci Methods*. 1999;94:93-103
41. Seth AK, Barrett AB, Barnett L. Granger causality analysis in neuroscience and neuroimaging. *J Neurosci*. 2015;35:3293-3297.
42. Tadel F, Baillet S, Mosher JC, Pantazis D, Leahy RM. Brainstorm: A user-friendly application for MEG/EEG analysis. *Comput Intell Neurosci*. 2011;2011:879716.
43. De Macedo Rodrigues K, Ben-Avi E, Sliva DD, et al. A FreeSurfer-compliant consistent manual segmentation of infant brains spanning the 0–2 year age range. *Front Hum Neurosci*. 2015;9:21.
44. Matarrese MAG, Loppini A, Jahromi S, et al. Electric source imaging on intracranial EEG localizes spatiotemporal propagation of interictal spikes in children with epilepsy. *Annu Int Conf IEEE Eng Med Biol Soc*. 2021;2021:2668-2671.
45. Sammaritano M, Luigi Gigli G, Gotman J. Interictal spiking during wakefulness and sleep and the localization of foci in temporal lobe epilepsy. *Neurology*. 1991;41(2):290-290.
46. Dimakopoulos V, Gotman J, Stacey W, et al. Protocol for multi-centre comparison of interictal high-frequency oscillations as a predictor of seizure freedom. *Brain Commun*. 2022;4:fcac151.
47. Ono M, Kubic S, Abernathy CD. In: Yasargil MG, ed. *Atlas of the cerebral sulci*. 1st ed. George Thieme; 1990
48. Tamilya E, Matarrese MAG, Ntolkeras G, et al. Noninvasive mapping of ripple onset predicts outcome in epilepsy surgery. *Ann Neurol*. 2021;89:911-925.
49. Kim D, Joo EY, Seo DW, et al. Accuracy of MEG in localizing irritative zone and seizure onset zone: Quantitative comparison between MEG and intracranial EEG. *Epilepsy Res*. 2016;127:291-301.
50. Engel J Jr. Surgery for seizures. *N Engl J Med*. 1996;334:647-653.
51. Scheuer ML, Wilson SB, Antony A, Ghearing G, Urban A, Bagić AI. Seizure detection: Interreader agreement and detection algorithm assessments using a large dataset. *J Clin Neurophysiol*. 2021;38:439-447.
52. Tamilya E, Park EH, Percivati S, et al. Surgical resection of ripple onset predicts outcome in pediatric epilepsy. *Ann Neurol*. 2018;84:331-346.
53. Gramfort A, Papadopoulos T, Olivi E, Clerc M. OpenMEEG: Opensource software for quasistatic bioelectromagnetics. *Biomed Eng Online*. 2010;9:45.
54. Dale AM, Liu AK, Fischl BR, et al. Dynamic statistical parametric mapping: Combining Fmri and MEG for high-resolution imaging of cortical activity. *Neuron*. 2000;26:55-67.
55. Perucca P, Dubeau F, Gotman J. Intracranial electroencephalographic seizure-onset patterns: Effect of underlying pathology. *Brain*. 2014;137:183-196.
56. Bartolomei F, Lagarde S, Wendling F, et al. Defining epileptogenic networks: Contribution of SEEG and signal analysis. *Epilepsia*. 2017;58:1131-1147.
57. Rolls ET, Huang CC, Lin CP, Feng J, Joliot M. Automated anatomical labelling atlas 3. *Neuroimage*. 2020;206:116189.
58. Bressler SL, Seth AK. Wiener–granger causality: A well established methodology. *Neuroimage*. 2011;58:323-329.
59. Marks DA, Katz A, Booke J, Spencer DD, Spencer SS. Comparison and correlation of surface and sphenoidal electrodes with simultaneous intracranial recording: An interictal study. *Electroencephalogr Clin Neurophysiol*. 1992;82:23-29.
60. Spencer SS. Cortical and intercortical seizure spread. In: Meldrum BS, Ferrendelli JA, Wieser HG, eds. *Current problems in epilepsy anatomy of epileptogenesis*. Vol 6. John Libbey; 1988:139-154.
61. Wieser HG. Human limbic seizures: EEG studies, origin and patterns of spread. In: Meldrum BS, Ferrendelli JA, Wieser HG, eds. *Current problems in epilepsy anatomy of epileptogenesis*. Vol 6. John Libbey; 1988:127-138.
62. Lai Y, Van Drongelen W, Hecox K, Frim D, Kohrman M, He B. Cortical activation mapping of epileptiform activity derived from interictal EcoG spikes. *Epilepsia*. 2007;48:305-314.
63. Spencer SS, Goncharova II, Duckrow RB, Novotny EJ, Zaveri HP. Interictal spikes on intracranial recording: Behavior, physiology, and implications. *Epilepsia*. 2008;49:1881-1892.
64. González Otárola KA, von Ellenrieder N, Cuello-Oderiz C, Dubeau F, Gotman J. High-frequency oscillation networks and surgical outcome in adult focal epilepsy. *Ann Neurol*. 2019;85:485-494.
65. Zhang M, Ladas TP, Qiu C, Shivacharan RS, Gonzalez-Reyes LE, Durand DM. Propagation of epileptiform activity can be independent of synaptic transmission, gap junctions, or diffusion and is consistent with electrical field transmission. *J Neurosci*. 2014;34:1409-1419.
66. Stefan H, da Silva FHL. Epileptic neuronal networks: Methods of identification and clinical relevance. *Front Neurol*. 2013;4:8.
67. Coben R, Mohammad-Rezazadeh I. Neural connectivity in epilepsy as measured by granger causality. *Front Hum Neurosci*. 2015;9:194.
68. Stone SSD, Park EH, Bolton J, et al. Interictal connectivity revealed by granger analysis of stereoelectroencephalography: Association with ictal onset zone, resection, and outcome. *Neurosurgery*. 2022;91:583-589.
69. Wilke C, van Drongelen W, Kohrman M, He B. Identification of epileptogenic foci from causal analysis of EcoG interictal spike activity. *Clin Neurophysiol*. 2009;120:1449-1456.
70. Varotto G, Tassi L, Franceschetti S, Spreafico R, Panzica F. Epileptogenic networks of type II focal cortical dysplasia: A stereo-EEG study. *Neuroimage*. 2012;61:591-598.
71. Van Mierlo P, Carrette E, Hallez H, et al. Ictal-onset localization through connectivity analysis of intracranial EEG signals in patients with refractory epilepsy. *Epilepsia*. 2013;54:1409-1418.
72. Coito A, Biethahn S, Tepperberg J, et al. Interictal epileptogenic zone localization in patients with focal epilepsy using electric source imaging and directed functional connectivity from low-density EEG. *Epilepsia Open*. 2019;4:281-292.
73. Guevara Erra R, Li K, Antonio Baccala L, et al. Dynamic network connectivity analysis to identify epileptogenic zones based on stereoelectroencephalography. *Front Comput Neurosci*. 2016;10:113.
74. Vlachos I, Krishnan B, Treiman DM, Tsakalis K, Kugiumtzis D, Iasemidis LD. The concept of effective inflow: Application to interictal localization of the epileptogenic focus from iEEG. *IEEE Trans Biomed Eng*. 2017;64:2241-2252.
75. Li YH, Ye XL, Liu QQ, et al. Localization of epileptogenic zone based on graph analysis of stereo-EEG. *Epilepsy Res*. 2016;128:149-157.
76. Coito A, Plomp G, Genetti M, et al. Dynamic directed interictal connectivity in left and right temporal lobe epilepsy. *Epilepsia*. 2015;56:207-217.
77. Numata-Uematsu Y, Uematsu M, Sakuraba R, et al. The onset of interictal spike-related ripples facilitates detection of the epileptogenic zone. *Front Neurol*. 2021;12:724417.
78. Jacobs J, Zijlmans M, Zelmann R, et al. High-frequency electroencephalographic oscillations correlate with outcome of epilepsy surgery. *Ann Neurol*. 2010;67:209-220.
79. Bartolomei F, Trébouchon A, Bonini F, et al. What is the concordance between the seizure onset zone and the irritative zone? A SEEG quantified study. *Clin Neurophysiol*. 2016;127:1157-1162.